J Mater Sci: Mater Electron (2023) 34:1461

Preparation and characterization of Cu-In-Ga-Se thin films by the electrodeposition technique using different metal salts and substrates

Arelis Ledesma-Juárez[1] and A. M. Fernández[1,*]

[1] *Instituto de Energías Renovables, Universidad Nacional Autónoma de México, Av. Xochicalco S/N, 62580 Temixco, Morelos, México*

Received: 17 January 2023
Accepted: 29 May 2023
Published online: 3 July 2023

ABSTRACT

$Cu(In, Ga)Se_2$ thin films possess important optoelectronic properties desirable for their application in devices such as solar cells. Solar cells based on this material have reached higher efficiencies than 23%. However, the commercialization of these cells has been restricted due to the use of thin film deposition methods involving costly high vacuum and cost. To reduce costs, it is necessary to use methods that do not use a high vacuum, among which electrodeposition stands out. Unfortunately, solar cells produced with this technique have yet to achieve high conversion efficiencies. Several authors attribute the lower efficiencies in such cells to the use of chemical additives in the preparation, different substrates, different deposition temperatures, etc. Nevertheless, there are very few reports on the influence of other metal salts in electrolytic baths. This work aims to use three different types of metal salts and voltages to produce $Cu(In, Ga)Se_2$ (CIGS) absorber thin films by co-electrodeposition technique. The effect of nucleation type with two different substrates is studied, also report the studies carried out on the atomic composition and structural, morphological, and electrochemical characterization to understand the formation, growth, and morphology of CIGS films and, in this way, to obtain a suitable stoichiometry of thin film solar cells using this absorber.

1 Introduction

The electrodeposition technique has shown great feasibility for the large-scale production of thin films $Cu(In, Ga)Se_2$ and, thus, the possible reduction in the production cost of solar cells based on this type of absorbers [1–3]. To increase the photovoltaic performance of these films, the following strategies had been: (i) the co-electrodeposition of $Cu(In, Ga)Se_2$ using an electrolyte, (ii) the electrodeposition of stacked layers of metals, alloys, or binary selenides, and (iii) the electroless technique. Each requires optimizing the film formation process by using additives, varying the deposition temperature, a

Address correspondence to E-mail: afm@ier.unam.mx

https://doi.org/10.1007/s10854-023-10745-8

complexing agent for the electrolyte solution, or varying concentrations of the salts used. Remarkably, the co-electrodeposition technique requires that the film's elements are reduced to the same potential so that they co-electrodeposit simultaneously, forming a thin film. This control is achieved through the complexation of metal ions and preferably maintaining a low pH of 1.5–3, as seen in [4]. In this regard, sodium sulfamate was also employed, which allowed the ratio of (Cu + Se)/ (In + Ga) to decrease. At the same time, the gallium content increased, and the film composition transformed from Cu-rich to Cu-poor [5]. The use of complexing agents such as KCN influences the reduction potentials of Cu^{2+} and Ga^{3+} relative to the uncomplexed species [6]. Using potassium sodium tartrate as a complexing agent for In ions and trisodium citrate for Ga ions allows the electrodeposition of In–Se and Ga–Se thin films in highly alkaline solutions [7]. In the case, In-Se, a coating efficiency of 68% had obtained at pH 13. Chelating agents form complexes, such as Triethanolamine (TEA) and Diethanolamine (EDTA), citric acid or trisodium citrate, sodium tartrate, and tartaric acids with Cu, In, and Ga ions. Under this strategy of electrodeposition of Cu-In-Ga oxide/hydroxide precursor films, the mass transfer-controlled deposition of the three elements had carried out, allowing control of the film composition. Reduction of the layer is carried out in a pure hydrogen atmosphere, allowing the formation of a mixture of In and $Cu_9(In, Ga)_4$. Using pure hydrogen instead of an Argon/Hydrogen mixture, the depletion of Ga due to the formation of $GaMo_3$ on the back side avoid, allowing the form construction of the $CuIn_{0.85}Ga_{0.15}Se_2$ phase [3]. Flexible substrates [8], various types of doping [9], as well as different types of metal layers [10–12], have been used by this technique. However, there are few studies on various types of metal salts. Some of these industry strategies have allowed for reaching efficiencies between 14 and 17% [13]. Nonetheless, the most attractive technique is co-electrodeposition, which uses an electrolyte solution and allows for optimizing the atomic composition of each metal. The main challenge in this technique is to obtain in a single step the CIGS film with an adequate polycrystallinity, a ratio of 0.93 for [Cu]/[In + Ga], and 0.3 for [Ga]/[In + Ga] [14], among other characteristics. In this work, we propose using three different types of metal salts to prepare thin films by co-electrodeposition technique and study the effect of the type of nucleation on two substrates (Molybdenum (Mo) and Fluorine Tin Oxide glass (FTO). Likewise, the different structural, morphological, atomic composition, and electrochemical characterization studies have shown a suitable stoichiometry for constructing solar cells based on $Cu(In, Ga)Se_2$ as an absorber.

2 Experimental section

2.1 Materials and equipment

Table 1 shows the molar concentration of each metal salt used in the preparation of each electrolytic bath and the type of substrate used. The purity and brand of each of the salts are copper(II) chloride dihydrate (99.99%), indium (III) chloride (99.999%), anhydrous gallium (III)chloride (99.99%), lithium chloride (≥ 99%), copper(II) nitrate hydrate (99. 999%), indium(III) nitrate hydrate (99.999%), gallium(III) nitrate hydrate (99.9%), lithium nitrate (99.99%), copper(II) sulfate (≥ 99%), indium(III) sulfate hydrate (99.99%), gallium(III) sulfate (99.99%), selenious acid (99.999%). The chemicals used were Aldrich Chemical Co, lithium sulfate reagent (99.7%), hydrochloric acid 37.4% ACS, nitric acid 70% ACS purchased from Fermont Company, and sulfuric acid 97.4% ACS from J.T. Baker, pH three buffer solutions from Hydrion Company.

The substrates used were FTO from Delta Technologies. The Mo substrate on glass had prepared in-house using direct current sputtering equipment, model Balzer BAE 250, with a Mo target of 5.08 cm.

2.2 Electrodeposition

CIGS films were fabricated by co-electrodeposition, using the reagents and molar composition indicated in Table 1, using the equipment Bio-Logic SAS

Table 1 The molar concentration of each of the salts used in the electrolytic baths

Bath no	2.6 (mM)	4.5 (mM)	10 (mM)	8 (mM)	1 (mM)
1	$CuCl_2$	$InCl_3$	$GaCl_3$	H_2SeO_3	LiCl
2	$Cu(NO_3)_2$	$In(NO_3)_3$	$Ga(NO_3)_3$	H_2SeO_3	$LiNO_3$
3	$CuSO_4$	$In_2(SO_4)_3$	$Ga_2(SO_4)_3$	H_2SeO_3	Li_2SO_4

potentiostat model VSP s/n: 0332 controlled with Ec-lab software was used to prepare the films.

2.3 Characterization

For analyzing the crystal structure, X-ray diffraction patterns of the films were recorded on DMAX-2200 with copper Kα radiation (λ_{Cu} = 1.5406 Å), and the X-ray beam was at 0.5° grazing incidence (GIXRD). The crystal size was estimated from the Scherrer Eq. (1) [17, 18]

$$D = \frac{K\lambda}{\beta \cos\theta} \quad (1)$$

where D is the average size of the crystals, K is the shape factor or so-called Scherrer constant = 1, λ is the wavelength of the X-ray equipment (Kα Cu) = 1.54 Å, β: width of the average height in radians (value of FWHM), θ: Bragg angle.

The atomic compositions of the films were obtained by EDS technique using Hitachi microscope model SU1510 SEM, which has a secondary electron detector and an energy dispersive X-ray detector model INCA-x-act. An electron accelerating voltage of 8 kV and energy emission levels $K\alpha$ for copper, selenium, gallium, and $L\alpha$ for indium had used to quantify the atomic composition. Atomic composition values were quantified over 600 µm × 600 µm. Micrographs of the films had obtained using a Hitachi model S-5500 SEM microscope with a secondary electron detector. An Alpha-step 100 profilometer had used for thickness measurement. Diffuse reflectance spectra obtained by UV–VIS measurement were performed using a Jasco V-670 spectrophotometer with a 2500–250 nm wavelength range.

The diffuse reflectance spectra data to equivalent absorption spectra by the Kubelka–Munk equation [15, 16]. The band gap of thin films and the equivalent absorption coefficient had related through the following Eq. (2):

$$\alpha h\upsilon = A\left(h\upsilon - E_g\right)^n \quad (2)$$

where α is the linear absorption coefficient, A is an arbitrary constant, $h\upsilon$ is the photon energy, and n equals 1/2 for direct transition-allowed materials.

The electrochemical techniques used were Cyclic Voltammetry (CV) and Chronoamperometry (CA), for electrodeposits and part of the characterization of CIGS films, employing a three-electrode cell, where the working electrode (WE) was FTO or Mo on glass (soda glass). The Mo film thickness was 1–2 microns and an active area of 1 cm × 3 cm. The counter electrode (CE) was a platinum mesh, and another platinum mesh was a reference electrode (REF). Ag/AgCl electrode had used as the reference electrode for CV. The potentiostat mode had used to prepare the CIGS films at three potentials -0.8, -0.9, and -1.0 V. The sweep rates used for the CV studies were 5 mVs^{-1}, 10 mVs^{-1}, and 20 mV s^{-1}.

3 Results and discussion

3.1 X-ray diffraction

Figure 1 shows the X-ray diffraction patterns of the CIGS films deposited from electrolytes containing the salts of the three metal ions Cu(II), In(III), and Ga(III), each of this with three different anions: patterns in (a), (b), and(c) are of films deposited on Mo using the chlorides, nitrates, and sulfates, respectively. and the patterns in (d), (e), and (f) are of the films deposited on FTO from the electrolytic baths prepared with the chlorides, nitrates, and sulfates, respectively, Figure 1a, b, and c shows a diffraction peak at 2θ = 40, which is attributable to the reflection from the (110) plane of the Mo substrate with a cubic structure with the lattice parameter a = 3.1472 Å (PDF#42-1120). The most intense diffraction peak observed in Fig. 1d, e, and f is due to reflection from the (112) plane of FTO. The other peaks observed in Fig. 1a–f, match the peaks reported as corresponding to reflections from the principal planes (112), (220), and (116) of $CuGa_{0.3}In_{0.7}Se_2$ phase (PDF#35-1102). These results show that the films deposited on both substrates, irrespective of the anion of the metal salt used in the electrolytic baths, are of the same phase $CuGa_{0.3}In_{0.7}Se_2$. Table 2 lists the principal planes along with the crystal size (ranging from 5 to 16 nm) estimated from the Scherrer equation [17, 18] in the case of each of these films. Thus, the X-ray diffraction data show that there is no significant change in the formation of the diffraction planes or the crystalline phase deposited using the different voltages applied and the anions present in the electrolytic baths.

3.2 Atomic composition by EDS

Tables 3a and b show the atomic composition results from EDS analyses of the films deposited under

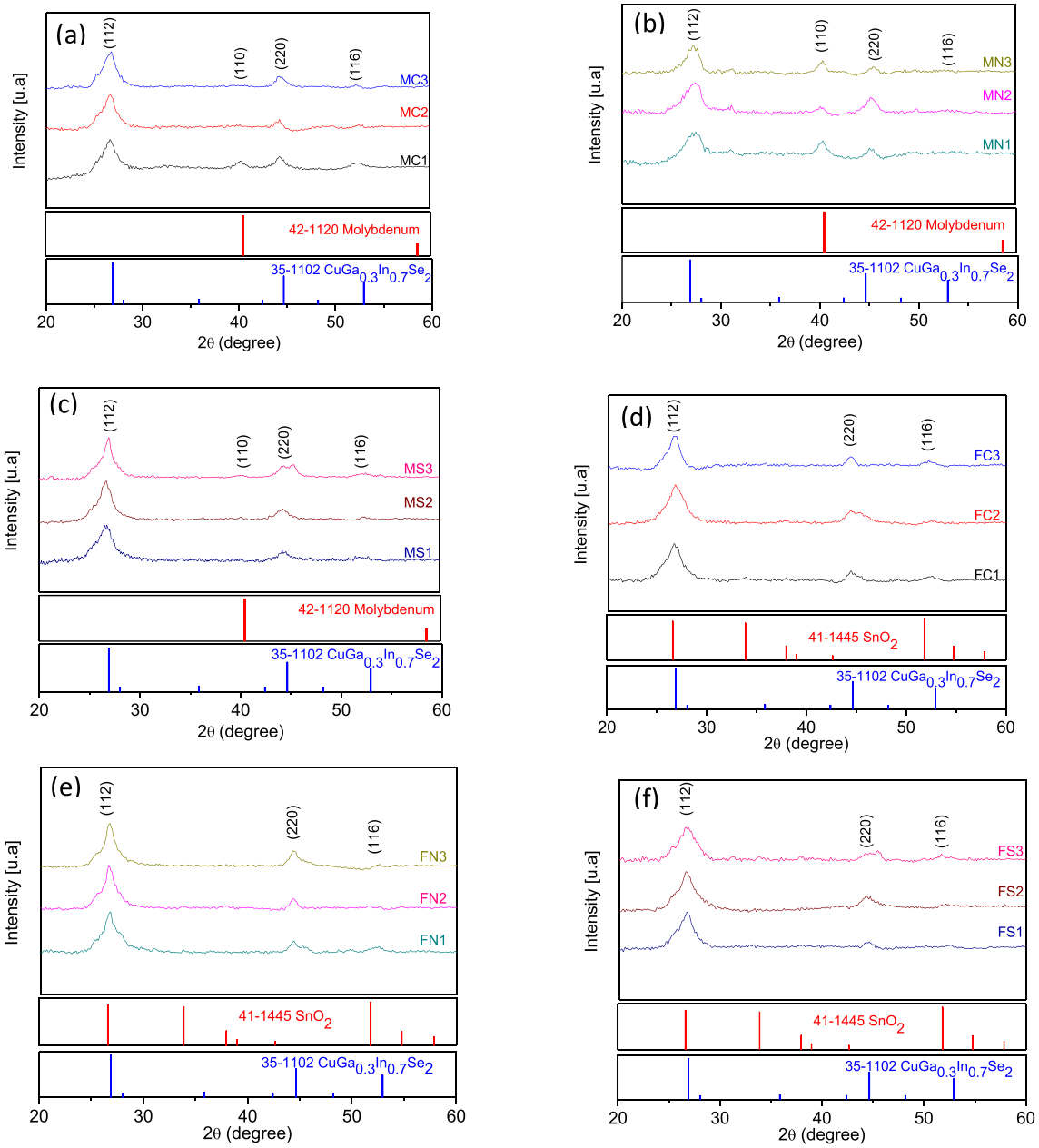

Fig. 1 X-ray diffraction spectra of the CIGS films, **a**, **b** and **c** correspond to the films deposited on Mo, using electrolytic baths of chlorides, nitrates, and sulfates, respectively, and **d** **e** and **f** correspond to the films deposited on FTO, using electrolytic baths of chlorides, nitrates, and sulfates respectively

different applied potentials: for example, MC1, MN1, MS1, FC1, FN1, and FS1, correspond to the films obtained using an applied voltage of − 1.0 V, while MC2, MN2, MS2, FC2, FN2, and FS2, as well as MC3, MN3, MS3, FC3, FN3, and FS3, to those obtained with the applied voltages of − 0.9 and − 0.8 V, respectively. Table 3 shows the compositions of the films deposited on Mo/glass substrates, and Table 4, that of those on FTO substrates. For efficient solar cells based on Cu-In-Ga-Se, the desirable atomic ratios are [Cu]/[In + Ga] ≈ 0.9 and [Ga]/[In + Ga] ≈ 0.3 [14]. In this sense, the values of [Cu]/[In + Ga] obtained for the films from the various electrolytic baths with nitrates, sulfates, and chlorides on Mo/glass substrate are high, higher than the optimum value of 0.9 (Table 3). When using FTO substrate, the samples prepared with chloride salts show these values higher than 0.9, while those with nitrates and sulfates

Table 2 Crystal size was estimated from the Scherrer equation, using the highest intensity plane of each sample and the main planes of each of the samples

Mo substrate		FTO substrate	
Sample	Crystal size (nm)	Sample	Crystal size (nm)
MC1	8	FC1	9
MC2	11	FC2	5
MC3	7	FC3	11
MN1	16	FN1	9
MN2	6	FN2	11
MN3	10	FN3	9
MS1	8	FS1	10
MS2	7	FS2	8
MS3	7	FS3	5

have a ratio lower than this value. In contrast, the [Ga]/[In + Ga] are similar to the theoretical value for all the samples from the chloride bath and the samples from the nitrate baths (MN1 and MN2). These results indicate that the Ga content in these samples is adequate, but the Cu content is much higher than the des. These are repeated for samples FC1, FC2, and FC3, however with both these atomic ratios reduced were the case of samples obtained with nitrate and sulfate baths on the FTO substrates, as shown in Table 4. Thus, the films deposited on Glass/Mo and FTO from an electrolytic bath based on chloride salts are close to the ideal atomic ratio values for the construction of thin film solar cells using Cu-In-Ga-Se as an absorber.

Table 3 Percentage values of the atomic composition for Ga/(In + Ga) and Cu/(In + Ga) ratios, obtained by EDS of CIGS films using Mo as substrate

Samples	Atomic values (% At.)						Thickness (μm)
	Cu	In	Ga	Se	Cu/(In + Ga)	Ga/(In + Ga)	
Mo-chlorides							
MC1	26.9	15.6	6.1	51.4	1.2	0.3	1.0
MC2	28.1	15.8	5.5	50.6	1.3	0.3	1.0
MC3	29.1	12.8	5.4	52.7	1.6	0.3	0.9
Mo-nitrates							
MN1	40.8	7.7	3.1	48.4	3.8	0.3	0.7
MN2	38.8	9.8	3.9	47.4	2.8	0.3	1.0
MN3	20.8	30.2	1.4	47.6	0.7	0.0	1.0
Mo-sulfates							
MS1	27.2	22.9	1.3	48.7	1.0	0.0	1.1
MS2	42.2	12.7	0.7	44.1	3.1	0.1	2.4
MS3	41.6	14.0	1.4	43.0	2.8	0.1	1.7

Table 4 Percentage values of the atomic composition for Ga/(In + Ga) and Cu/(In + Ga) ratios, obtained by EDS of CIGS films using FTO as substrate

Sample	Atomic values (at. % At.)						Thickness (μm)
	Cu	In	Ga	Se	Cu/(In + Ga)	Ga/(In + Ga)	
FTO-cloruros							
FC1	26.2	14.5	6.1	53.2	1.3	0.3	0.7
FC2	38.4	7.2	4.8	49.6	3.2	0.4	1.0
FC3	31.0	12.0	5.0	51.9	1.8	0.3	0.9
FTO-nitrates							
FN1	17.5	17.3	2.6	62.3	0.9	0.1	0.8
FN2	13.4	23.1	2.2	61.3	0.5	0.1	0.9
FN3	14.6	17.0	3.6	64.7	0.7	0.1	0.8
FTO-sulfates							
FS1	17.1	32.4	0.5	50.8	0.5	0.0	0.8
FS2	24.7	29.9	3.3	42.1	0.7	0.1	0.7
FS3	23.7	25.8	1.1	49.4	0.9	0.0	0.7

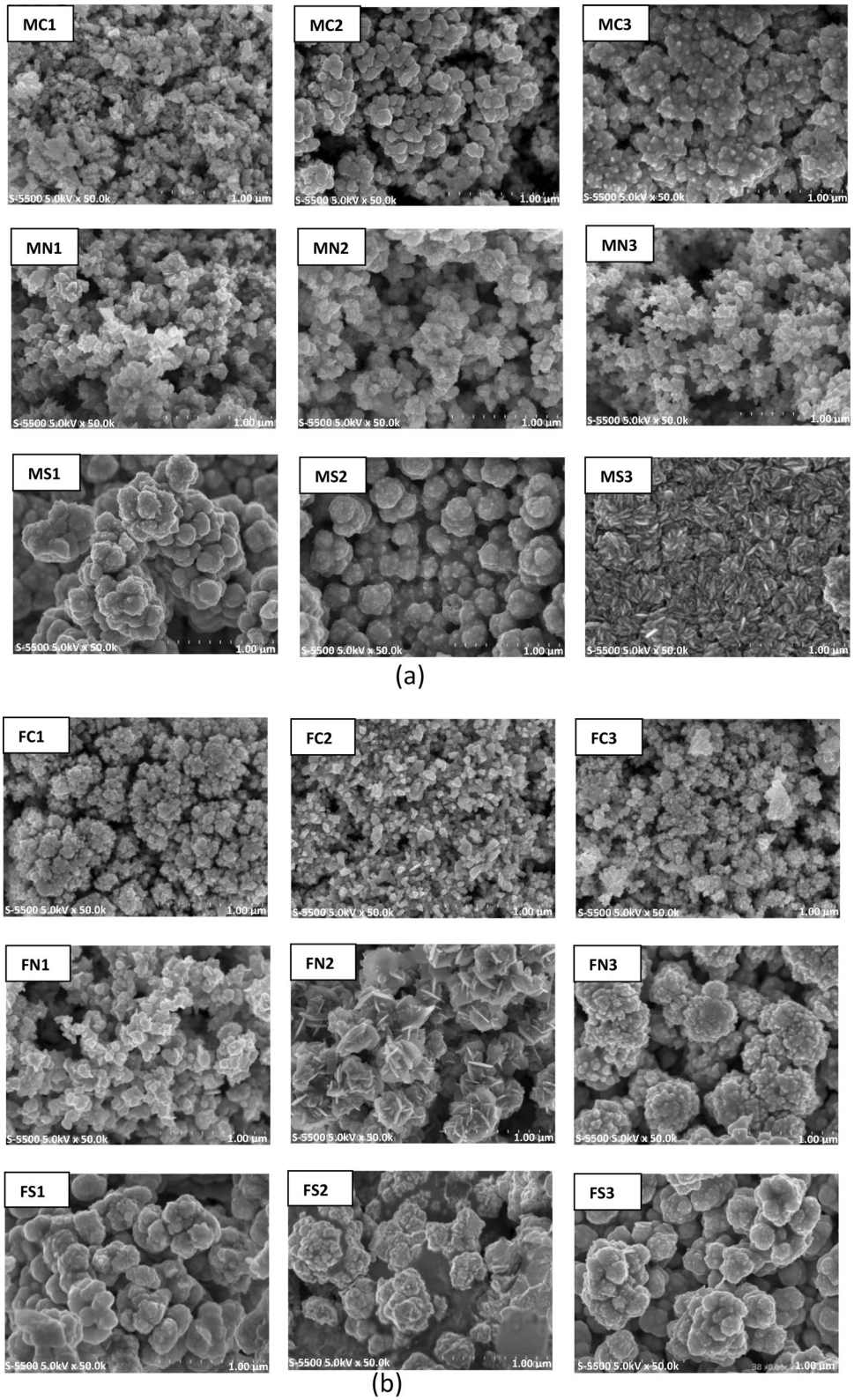

Fig. 2 Micrographs of the surface of CIGS films, fabricated using Mo (M) and FTO (F) as substrates, using various types of salts (chlorides (C), nitrates (N) or sulfates (S)) at overpotentials of − 1.0 V (1), − 0.9 V (2), or − 0.8 V (3)

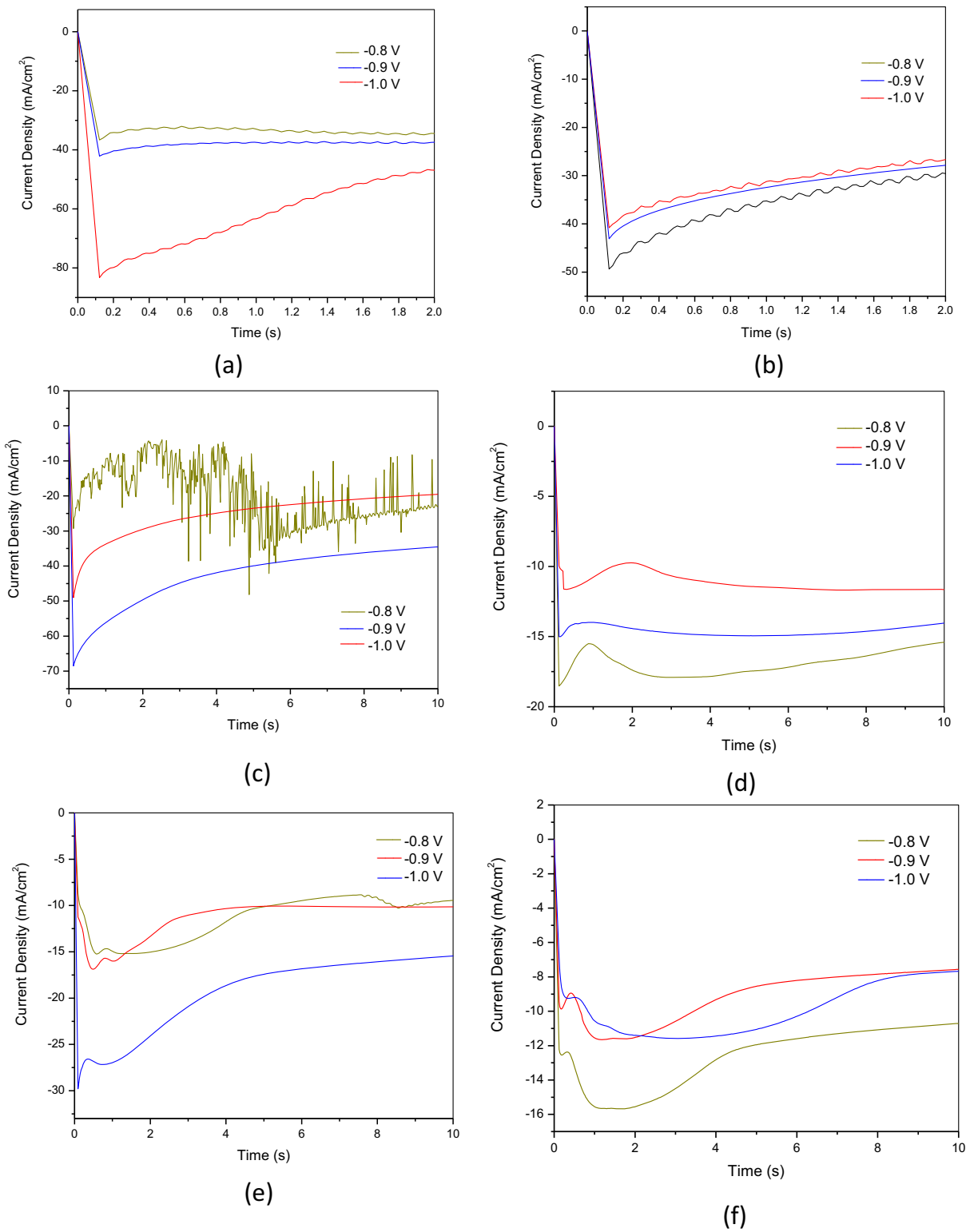

Fig. 3 Current density-time plots obtained during the electrodeposition of CIGS films using glass/Mo (**a**, **b** and **c**) and FTO (**d**, **e**, and **f**) substrates

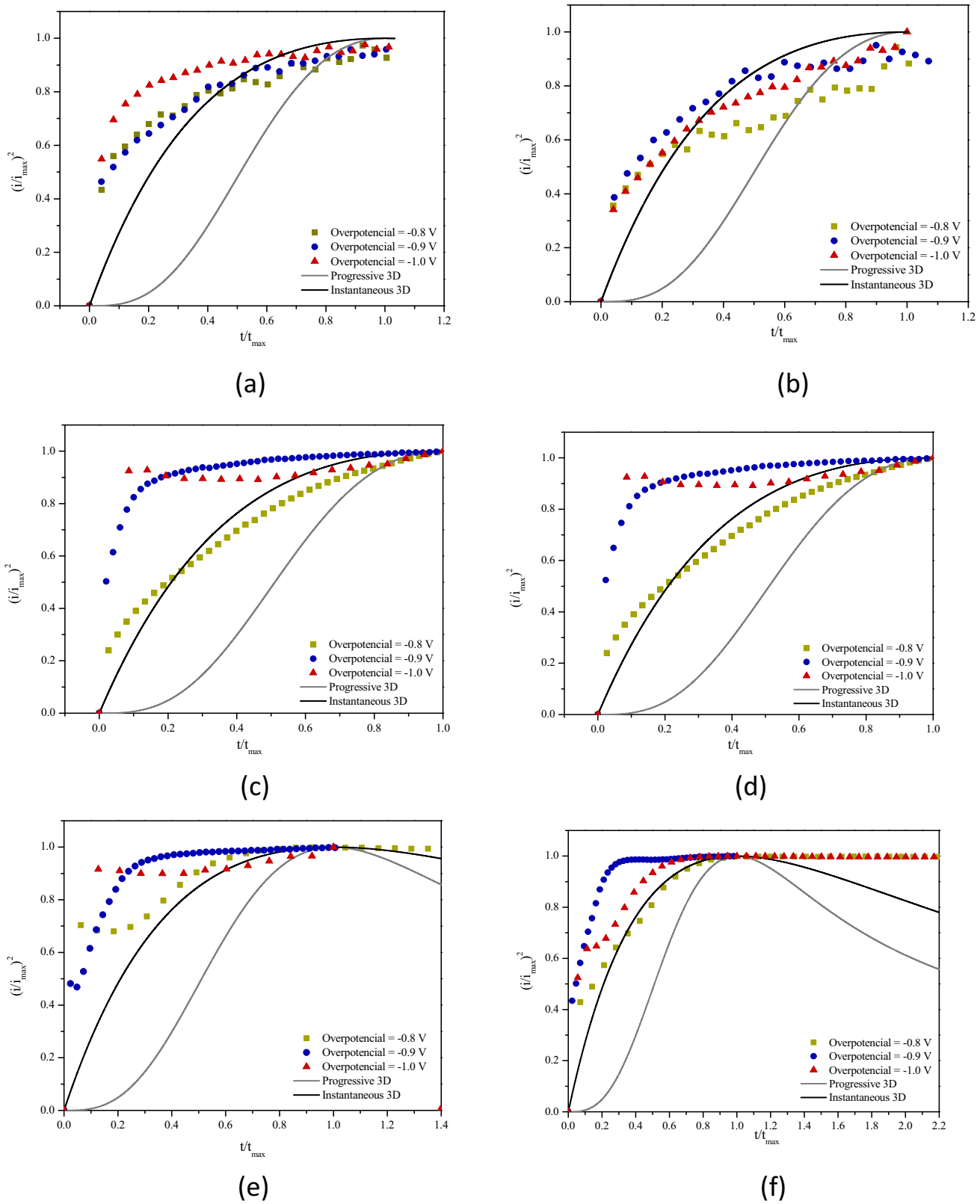

Fig. 4 **a**, **b** and **c** correspond to CIGS time–current transients using Molybdenum/glass as substrate and chloride, nitrate, and sulfate salts, respectively. **d**, **e** and **f** correspond to CIGS time–current transients using FTO as substrate and chloride salts, nitrates, and sulfates, respectively

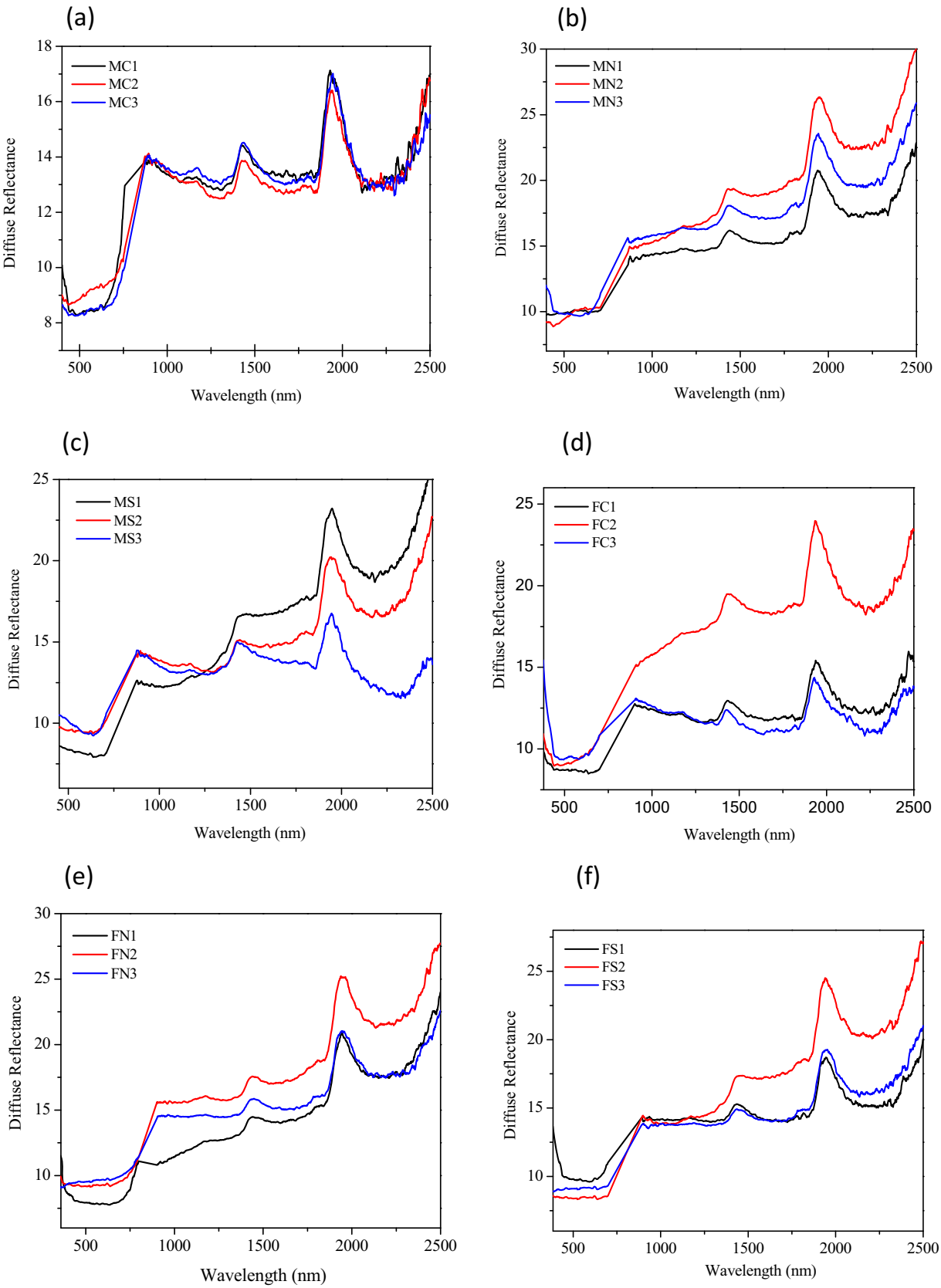
(a)
MC1
MC2
MC3
Diffuse Reflectance
Wavelength (nm)
(b)
MN1
MN2
MN3
Diffuse Reflectance
Wavelength (nm)
(c)
MS1
MS2
MS3
Diffuse Reflectance
Wavelength (nm)
(d)
FC1
FC2
FC3
Diffuse Reflectance
Wavelength (nm)
(e)
FN1
FN2
FN3
Diffuse Reflectance
Wavelength (nm)
(f)
FS1
FS2
FS3
Diffuse Reflectance
Wavelength (nm)

◀**Fig. 5** Diffuse reflectance spectra of CIGS films deposited on Molybdenum (**a**, **b**, and **c**) and FTO (**d**, **e**, and **f**) using chloride, nitrate, and sulfate salts, respectively

3.3 Scanning electron microscopy

Figures 2a and b show the morphology of CIGS samples obtained on Mo and FTO substrates, respectively. The SEM images show cauliflower-type growth; each cluster comprises grains ranging in size from 0.05 to 0.12 microns. The grain size is a function of the type of metal salt used, the applied voltage, and the type of substrate. For example, the SEM micrographs in Fig. 2a, that the films MC1, MC2, and MC3 have very similar granular growth with grain sizes of 0.07, 0.09, and 0.06 microns, respectively, the grain varying depending on the voltage applied for the deposition of the films. Similar behavior is observed in MN1 to MS3 films. In the case of samples MS1 and MS2, forming cauliflower-shaped clusters, the grain size is 0.13 and 0.12, respectively. MS3 shows the formation of scales on the spherical grains, most likely due to the possible formation of Cu-Se, as reported previously from elsewhere [19–22].

Figure 2b shows the morphology of the CIGS samples on an FTO-coated substrate. These samples show similar morphology to the pieces on a Mo substrate. The average grain size ranges from 0.03 to 0.07 microns. Samples FC1, FC2, and FC3 have smaller grains than samples MC1, MC2, and MC3. Samples obtained with a nitrate bath present small grains that agglomerate to form larger clusters, as seen in the SEM micrograph of the samples FN1 and FN3, since FN2 presents the formation of flakes whose dimensions are up to 0.10 microns. Samples FS1, FS2, and FS3, are formed by conglomerates of grains whose average size ranges between 0.07 and 0.09 microns. We also observed the formation of voids between these conglomerates in these micrographs. Thus, for all these samples, very similar granular growth is observed on the two types of substrates from the electrolytic solutions with the salts of different anions. However, the films grown on Mo/glass substrates have smaller grain sizes than those grown on FTO.

3.4 J–t transients

The growth of CIGS films is directly related to the applied overpotential, i.e., the development of these films carried out by the kinetic mechanism of nuclei growth. These mechanisms had described by the instantaneous and progressive nucleation equations of Scharifker and Hill [23], where I_{max} and t_{max} are the maximum current and t corresponds to the maximum current in the CTT (Current–Time Transient) growth and nucleation region,

3D Progressive nucleation

$$\left(\frac{i}{i_{max}}\right)^2 = \left(\frac{1.2254}{\frac{t}{t_{max}}}\right) \times \left[1 - exp\left(-2.3367\left(\frac{t}{t_{max}}\right)^2\right)\right]^2 \quad (3)$$

3D Instantaneous nucleation

$$\left(\frac{i}{i_{max}}\right)^2 = \left(\frac{1.9542}{\frac{t}{t_{max}}}\right) \times \left[1 - exp\left(-1.2564\left(\frac{t}{t_{max}}\right)\right)\right]^2 \quad (4)$$

Fig. 3a–f show the current density-time plots obtained during the electrodeposition of CIGS films using glass/Mo (a, b, and c) and FTO (d, e, and f) substrates. The observed increase in current is associated with an increase in the electroactive area and the stabilization and growth of new nuclei; subsequently, the observed slow decay is due to a mass transfer-controlled process. This behavior is characteristic of three-dimensional (3D) diffusion-controlled nucleation processes [24]. Figure 4a, b, and c compares the transient curves for the theoretical 3D-type progressive and instantaneous growth and those of CIGS on Mo substrates. In contrast, Fig. 4d, e, and f are for those on FTO substrates at three different applied overpotentials and using chloride, nitrate, and sulfate salts, respectively. The values obtained with these equations show a behavior very close to the 3D-instantaneous change for all samples. It also is mentioned that the FTO substrate is a favorite over glass/Mo substrates. The same type of growth has been reported on CIGS films using only chloride salt baths [25]. Therefore, the effect of the kind of growth, whether chlorides, nitrates, or sulfates, is influenced by the type of substrate, which will determine whether it is instantaneous or progressive style with a 3D growth rate.

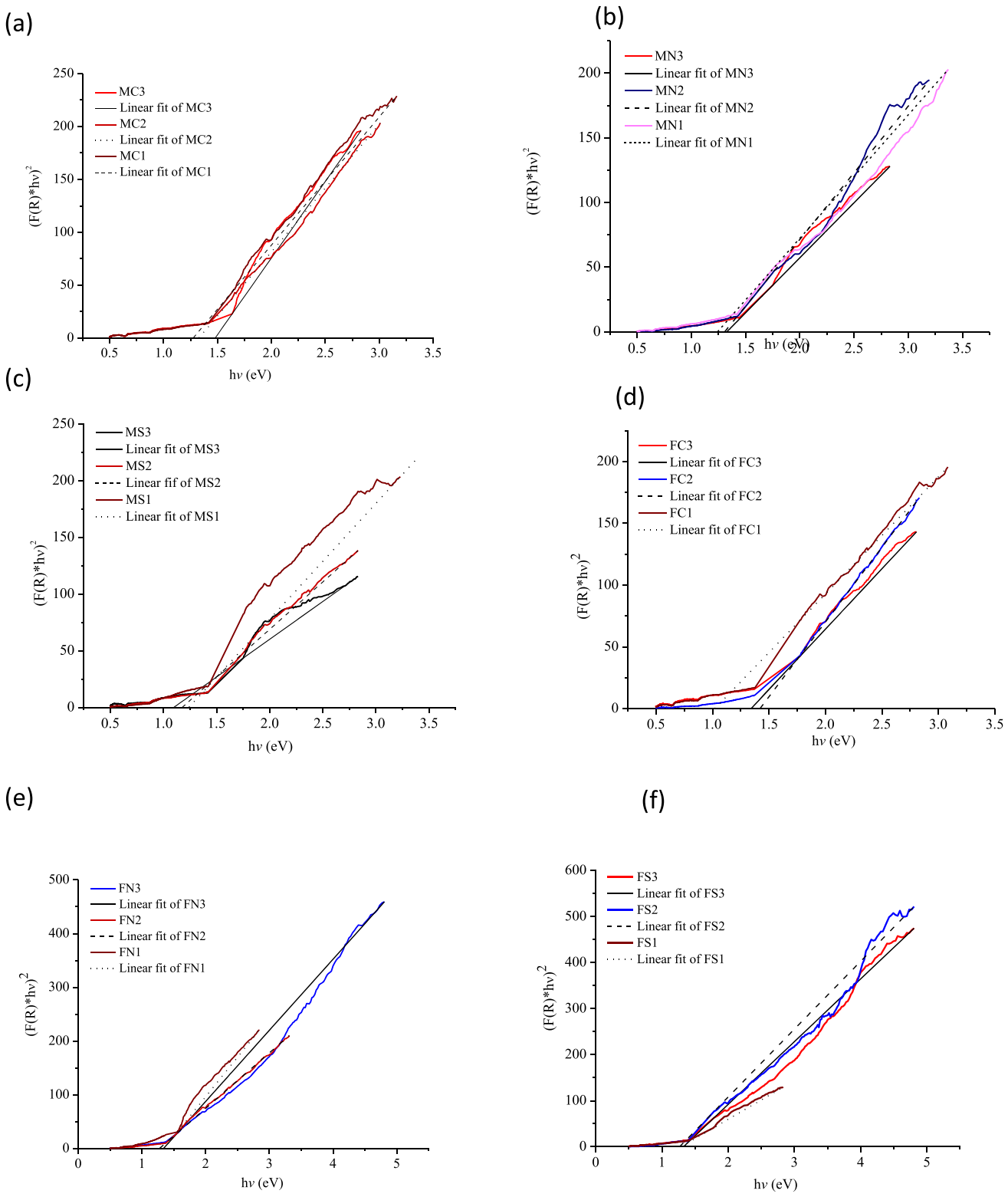

Fig. 6 Graphs obtained by the Kubelka-Mung method of CIGS films deposited on Molybdenum (**a**, **b**, and **c**) and FTO (**d**, **e**, and **f**), using chloride, nitrate, and sulfate salts, respectively, to calculate the band gap

Table 5 Bandwidth values for the CIGS films made with the electrolytic baths had shown in Table 1

Sample	Band gap value (eV)	Sample	Band gap value
MC1	1.27	FC1	1.02
MC2	1.32	FC2	1.42
MC3	1.47	FC3	1.34
MN1	1.24	FN1	1.33
MN2	1.30	FN2	1.27
MN3	1.32	FN3	1.34
MS1	1.24	FS1	1.28
MS2	1.17	FS2	1.26
MS3	1.09	FS3	1.32

3.5 Optical properties

Figure 5 shows the Diffuse reflectance spectra of CIGS films deposited on Molybdenum (a, b, and c) and FTO (d, e, and f), using chloride, nitrate, and sulfate salts, respectively. Figure 6 shows the different graphs obtained by applying the Kubelka-Mung method on the diffuse reflectance spectra of CIGS films deposited on Molybdenum (a, b, and c) and FTO (d, e, and f), from chloride, nitrate, and sulfate solutions. Table 5 lists the bandgap values obtained from such plots for the CIGS films deposited on molybdenum (Mo)-coated and FTO-coated substrates. The CIGS films on FTO show slightly higher bandgaps than those deposited on Mo. Further, the observed bandgaps are higher for the films deposited on Mo from the chloride or nitrate electrolytic baths, but not for those deposited from the sulfate baths. The band gap in CIGS films is reported to be close to 1.14 eV [26]. The differences in the observed bandgaps in the present films, Table 5, from the reported bandgap are probably due to the different voltage conditions and types of salts used for the film depositions, which influence the optoelectronic characteristics of the films. According to this table, the bandgap of the films on Mo substrates deposited from the chloride or nitrate bath decreases as the applied potential increases, while those for the films from the sulfate baths decrease with the decrease in voltage. When FTO substrates are used, there is no trend of increasing or decreasing bandgap values.

3.6 Electrochemical evaluation

Figures 7a–c and d–f show the voltammograms obtained by the cyclic voltammetry technique for the solutions prepared with metal salts (chlorides, nitrates, and sulfates), using glass/Mo and FTO as substrates at different scanning speeds of 5, 10, and 20 mV/s, respectively. As observed in Fig. 7a a reduction peak at − 0.726 V (vs. Ag/AgCl) is probably due to Ga deposition; likewise, another one had observed at an anodic potential of − 0.350 V (vs. Ag/AgCl), most likely due to Gallium oxidation. In addition, a potential crossover is approximately − 0.360 V due to the formation of a deposit on the Mo electrode surface, possibly Gallium. Figure 5b shows an anodic potential peak at approximately 0.35 and 0.75 V (vs. Ag/AgCl), probably due to oxidation of the Cu film formed. Nevertheless, the pH is acidic, and developing the precursor salts' Ga, In, and Li hydroxides on the electrode surface is possible [3].

Figure 7c shows three potential values associated with the reduction processes of Cu, In, and Ga elements; 0.012, − 0.096, and − 0.205 V (vs. Ag/AgCl), respectively, at the rate of 5 mV/s. At this rate, an anodic peak due to an oxidation process occurs at approximately − 0.307 V (vs. Ag/AgCl). At the rates of 10 and 20 mV/s, neither cathodic nor anodic peaks are observed; this is probably because the deposited Mo film was unstable in the presence of sulfates. Figure 7d shows a potential peak corresponding to a reduction process around -0.003 V (vs. Ag/AgCl), probably due to Cu reduction, and an oxidation process around 0.456 V (vs. Ag/AgCl), possibly to Cu. These processes had shown at the three sweep rates 5, 10, and 20 mV/s, which means that the FTO electrode surface is stable in the chloride salts. Figure 7e shows three potential peaks corresponding to reduction around − 0.055, − 0.254, and − 0.600 V (vs. Ag/AgCl), most likely Cu, Ga, and In deposits, respectively, and three oxidation processes observed at approximately 0.166, 0.432, and 677 V (vs. Ag/AgCl), attributed to Cu, Ga, and In elements. These processes appear at the three scan rates of 5, 10, and 20 mV/s, which means that the FTO electrode surface is more stable than Mo in the presence of nitrate salts. Figure 7f shows two potential peaks corresponding mainly to reduction at around − 0.083 and − 0.644 V (vs. Ag/AgCl), most likely deposited from Cu, Ga, respectively, and two oxidation processes observed at around -0.590 and 0.542 V vs. Ag/AgCl,

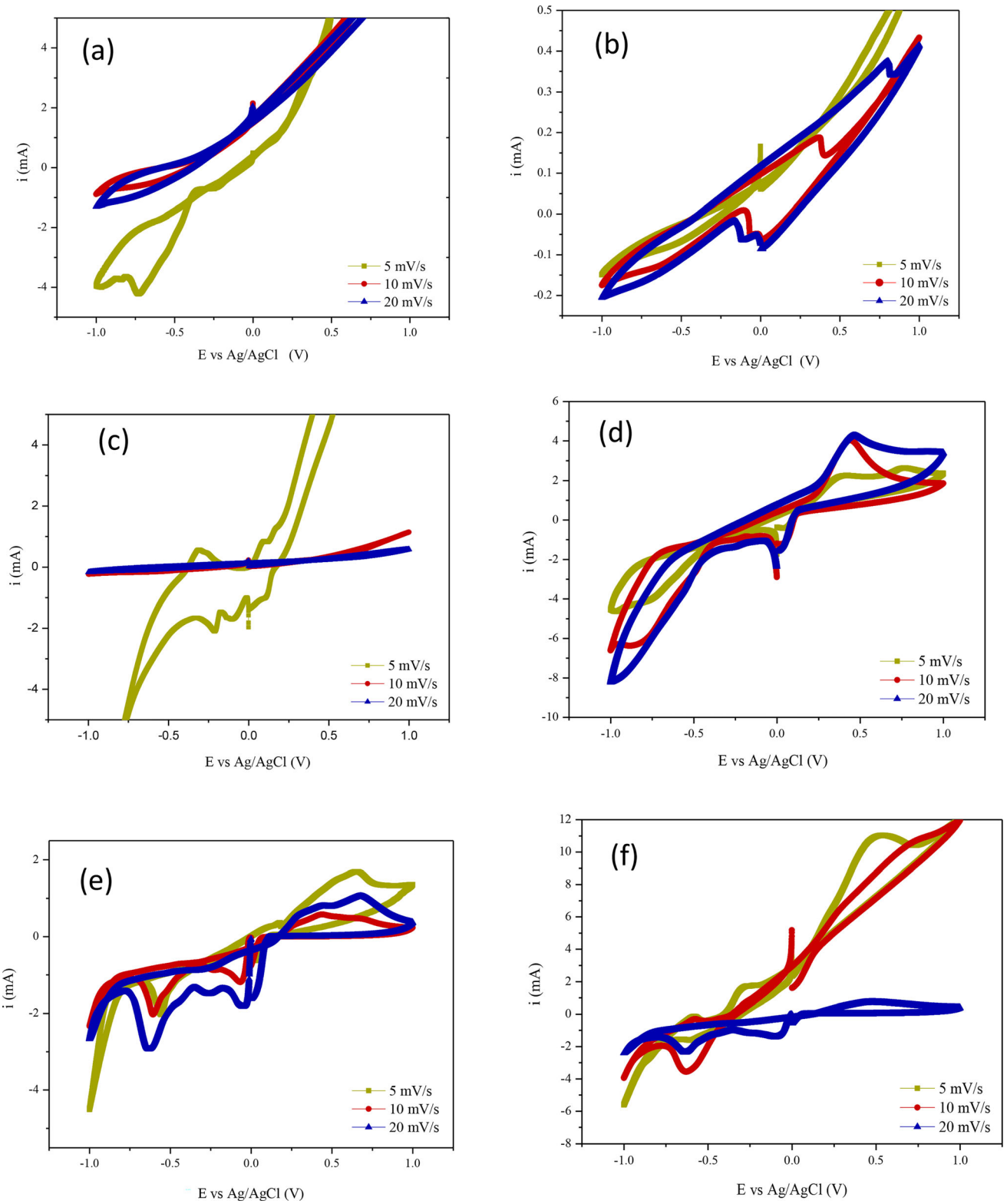

Fig. 7 Voltagrams of the CIGS electrolytic baths, using Mo (**a**, **c**, **e**) and FTO (**b**, **d**, **f**) as working electrodes using chloride, nitrate, and sulfate salts respectively, at 5 mV, 10 mV, and 20 mV each

attributed to Cu, Ga elements. These processes appear at all three sweep rates, 5, 10, and 20 mV/s, which means that the FTO electrode surface is less stable in sulfate salts than in nitrate salts.

4 Conclusion

Based on the EDS results, samples obtained from chloride salts on glass/Mo and FTO substrates show a Ga/(In + Ga) close to the ideal ratio of 0.3. When using electrolytic baths based on nitrate salts, similar values are obtained for MN1 and MN2 samples. Therefore, it is possible to indicate that the chloride-based bath favors the incorporation of Ga in the film. The main phase obtained corresponds to $CuGa_{0.3}In_{0.7}Se_2$ (PDF #35–1102), whose principal diffraction planes are (112), (220), and (116) for all prepared samples, regardless of the type of electrolytic bath used or the type of substrate, according to X-ray diffraction analysis. SEM analysis shows a morphology consisting of cauliflower-type for most of the CIGS samples. According to the models used to evaluate the type of growth, it is found that the nucleation process of the deposited films is instantaneous with a 3D development, which is more noticeable when FTO was used as substrate. The band gap values are low in the case of the CIGS films deposited on Mo-coated glass substrates but increase by increasing the applied overpotential when the electrodeposition baths are prepared using chloride and sulfate salts. According to the results of cyclic voltammetry, essential changes were observed when using different metal salts; for example, sulfate salts favor the formation of several reductions and oxidation peaks for Cu, In, and Ga, and in particular, using FTO substrates. On the contrary, the use of Mo substrates favors the reduction processes associated with each metal ion in particular in the chloride baths, which will select the electrodeposition of the three metals (Cu, In, Ga) in such a way as to favor the metal alloy that allows reacting with it, and thus the formation of the CIGS film.

Acknowledgements

This work was supported through project PAPIIT-IN111320. Arelis Ledesma-Juarez thanks CONACyT for the postdoctoral fellowship. We also thank María Luisa Ramón García for the XRD measurements, Rogelio Morán Elvira for the SEM measurements, and José Campos Álvarez for assistance in the EDS analysis.

Author contributions

All authors contributed to the study's conception and design. AL-J: performed material preparation, data collection, and analysis. AMF: wrote the first draft of the manuscript, and all authors commented on previous versions. All authors read and approved the final manuscript.

Funding

This work was partially supported by PAPIIT-IN111320. Author Arelis Ledesma-Juarez has received research support from CONACYT (Mexico) under Postdoctoral Program.

Data availability

The data supporting this study's findings are available from the corresponding author upon reasonable request.

Declarations

Conflict of interest The authors have no relevant financial or non-financial interests to disclose.

Ethical approval This article does not contain any studies involving animals performed by any authors. Also, this article has no studies involving human participants performed by authors.

References

1. S. Saha, M. Johnson, F. Altayaran, Y. Wang, D. Wang, Q. Zhang, Electrodeposition fabrication of chalcogenide thin films for photovoltaic applications. Electrochem **1**, 286–321 (2020). https://doi.org/10.3390/electrochem1030019
2. M.A. Green, E.D. Dunlop, D.H. Levi, H. Ebinger, J. Yoshita, A.W. Ho-Baillie, Solar cell efficiency tables. Prog. Photovoltaics **27**, 565–575 (2019). https://doi.org/10.1002/pip.3171
3. A. Duchatelet, T. Sidali, N. Loones, G. Savidand, E. Chassaing, D. Lincot, 12.4% Efficient Cu(In, Ga)S e2 solar cell prepared from one step electrodeposited Cu–In–Ga oxide precursor layer. Solar Energy Mater. Solar Cells **119**, 241–245 (2013). https://doi.org/10.1016/j.solmat.2013.07.053
4. V.S. Saji, C.-Y. Jung, C.-W. Lee, Electrodeposition of copper, selenium, indium, and gallium on molybdenum/surface oxides: unary, binary, ternary and quaternary compositions. J. Electrochem. Soc. **162**, D465–D479 (2015). https://doi.org/10.1149/2.0451509jes
5. J. Liu, F. Liu, Y. Lai, Z. Zhang, J. Li, Y. Liu, Effects of sodium sulfamate on electrodeposition of Cu(In, Ga)Se2 thin film. J. Electroanal. Chem. **651**, 191–196 (2011). https://doi.org/10.1016/j.jelechem.2010.10.021
6. J.J.J. Muthuraj, D.H. Rasmussen, I.I. Suni, Electrodeposition of CuGaSe2 from thiocyanate-containing electrolytes. J. Electrochem. Soc. **158**, D54 (2011). https://doi.org/10.1149/1.3519997
7. S. Aksu, M. Pinarbasi, Electrodeposition methods and chemistries for deposits precursor thin films deposition: 37th IEEE Photovoltaic Specialists Conference, Seattle, 2011. https://doi.org/10.1109/PVSC.2011.6185907
8. M. Pagliaro, R. Ciriminna, G. Palmisano, Flexible solar cells. Chemsuschem **1**, 880–891 (2008). https://doi.org/10.1002/cssc.200800127
9. P. Reinhard, B. Bissig, F. Pianezzi, E. Avancini, H. Hagendorfer, D. Keller, P. Fuchs, M. Döbeli, C. Vigo, P. Crivelli, S. Nishiwaki, S. Buecheler, A.N. Tiwari, Features of KF and NaF postdeposition treatments of Cu(In, Ga)Se_2 absorbers for high-efficiency film solar cells. Chem. Mater. **27**, 5755–5764 (2015). https://doi.org/10.1021/acs.chemmater.5b02335
10. R Kamada, T. Yagioka, S. Adachi, A. Handa, K. F. Tai, T. Kato, H Sugimoto, New world record Cu(In, Ga)(Se, S)$_2$ thin film solar cell efficiency beyond 22%. In: IEEE 43rd Photovoltaic Specialists Conference (PVSC), Portland, 2016. https://doi.org/10.1109/pvsc.2016.7749822.
11. P. Jackson, R. Wuerz, D. Hariskos, E. Lotter, W. Witte, M. Powalla, Effects of heavy alkali elements in Cu(In, Ga)Se_2 solar cells with efficiencies up to 22.6%. Phys. Status Solidi RRL **10**, 583–586 (2016). https://doi.org/10.1002/pssr.201600199
12. T.M. Friedlmeier, P. Jackson, A. Bauer, D. Hariskos, O. Kiowski, R. Wuerz, M. Powalla, Improved photocurrent in Cu(In, Ga) Se_2 solar cells: from 20.8% to 21.7% efficiency with CdS buffer and 21.0% Cd-free. IEEE J. Photovolt. **5**, 1487–1491 (2015). https://doi.org/10.1109/JPHOTOV.2015.2458039
13. V. Bermudez, NEXCIS CIGS technology: from R&D to industry, in Proceedings of the 4th International Workshop on CIGS Solar Cell Technology, 2013.
14. H. Lee, H. Yoon, H. Ji, D. Lee, J. Lee, J. Yun, A. Kim, Fabrication of CIGS films by electrodeposition method for photovoltaic cells. J. Electron. Mater. **41**(12), 3375–3381 (2012). https://doi.org/10.1007/s11664-012-2252-x
15. A. Escobedo Morales, E. Sanchez Mora, U. Pal, Use of diffuse reflectance spectroscopy for optical characterization of un-supported nanostructures. Rev. Mex. Fis. **53**(5), 18–22 (2007)
16. S.S. Abdullahi, S. Güner, Y. Koseoglu, I.M. Musa, B.I. Adamu y, M.I. Abdulhamid, Sımple method for the determination of band gap of a nanopowdered sample using Kubelka Munk theory. J. Nigerian Assoc. Math. Phys. **35**, 241–246 (2016)
17. U. Holzwarth, N. Gibson, The Scherrer equation versus the 'Debye-Scherrer equation.' Nat. Nanotechnol. **6**, 534 (2011). https://doi.org/10.1038/nnano.2011.145
18. H. Saïdia, C. Ben Alayaa, M.F. Boujmila, B. Durand, J.L. Lazzari, M. Bouaïcha, Physical properties of electrodeposited CIGS films on crystalline silicon: Application for photovoltaic hetero-junction. Curr. Appl. Phys. **20**, 29–36 (2020). https://doi.org/10.1016/j.cap.2019.09.015
19. R. Chandran, R. Pandey, A. Mallik, One step electrodeposition of $CuInSe_2$ from an acidic bath: a reduction co-deposition study. Mater. Lett. **160**, 275–277 (2015). https://doi.org/10.1016/j.matlet.2015.07.132
20. Y. Lai, F. Liu, Z. Zhang, J. Liu, S. Kuang, J. Lie, Y. Liu, Cyclic voltammetry study of electrodeposition of Cu(In, Ga)Se2 thin films. Electrochim. Acta **54**, 3004–3010 (2009)
21. T. Roldan, A.M. Blas, E.L. Cruz, M.E. Calixto, Semiconducting Cu_2Se thin films obtained by electrochemical deposition for possible applications in thermoelectric systems. MRS Adv. **7**, 1–4 (2002). https://doi.org/10.1557/s43580-021-00197-9

22. A. Moysiadou, R. Koutsikou, M. Bouroushian, Pulse electrodeposition of copper selenide from acidic aqueous baths. Mater. Lett. **139**, 112–115 (2015). https://doi.org/10.1016/j.matlet.20214.10.036
23. A. Guptay, C. Srivastava, Nucleation and growth mechanism of tin electrodeposition on graphene oxide: a kinetic, thermodynamic and microscopic study. J. Electroanal. Chem. **861**, 113964 (2020)
24. B. Scharifker, G. Hills, Theoretical and experimental studies of multiple nucleation electrochim. Acta **28**, 879–889 (1983)
25. F. Liu, C. Huang, Y. Lai, Z. Zhang, J. Li, Y. Liu, Preparation of Cu(In, Ga)Se_2 thin films by pulse electrodeposition. J. Alloy. Compd. **509**, L129–L133 (2011). https://doi.org/10.5772/intechopen.71857
26. J. Ramanujam, U.P. Singh, Copper indium gallium selenide based solar cells – a review. Energy Environ. Sci. **10**, 1306–1319 (2017). https://doi.org/10.1039/c7EE00826K